SIMULATION ANALYSIS AND EXPERIMENTAL STUDY OF THE ORCHARD VEHICLE-MOUNTED FLOWER-THINNING MACHINE
/
果园机载式疏花机的仿真分析与试验

Yuliang WANG [1,2], Bowen GUO [1,2], Zhaoying CHEN[1,2], Yuhao MA[1,2], Guoqiang FAN[1,2], Jinxing WANG [*1,2]
[1]College of Mechanical and Electronic Engineering, Shandong Agricultural University, Tai an 271018 / China;
[2]Shandong Provincial Key Laboratory of Horticultural Machinery and Equipment, Tai an 271018 / China;
Tel: +86 05388246826; E-mail: jinxingw@163.com
DOI: https://doi.org/10.35633/inmateh-78-51

Keywords: *Flower-thinning machine, simulation analysis, Box-Behnken design, parameter optimization*

ABSTRACT
Orchard flower thinning is essential for improving fruit quality and stabilizing yield in modern orchards, yet traditional manual and chemical methods no longer satisfy the demands of mechanized orchard management. To address the characteristics of China's dwarf and dense orchard planting system, a hydraulic-driven vehicle-mounted flower-thinning machine was developed. Dynamic simulations of the flower-thinning process were conducted using ANSYS/LS-DYNA to analyze the effects of thinning shaft rotational speed, traveling speed, and thinning radius on the striking force. A regression model for the striking force was established using single-factor experiments and a three-factor, three-level Box-Behnken design. The results showed that all three factors significantly influenced the striking force, with notable interaction effects. When the thinning radius was 0.4 m, the optimal operating parameters were a rotational speed of 290 r·min⁻¹ and a traveling speed of 5.4 km·h⁻¹, corresponding to an effective thinning range of 0.4–0.6 m. Under these conditions, the striking forces obtained from simulation and indoor bench tests were 5.083 N and 5.22 N, respectively, with a relative error of 2.7%. Field experiments further demonstrated an average thinning rate of 37.8% under the optimal parameters, achieving effective thinning while reducing damage to branches and leaves.

摘要
果园疏花作业是提升果实品质与稳定产量的关键环节，传统人工与化学疏花均难以满足现代果园管理需求。针对我国矮密果园种植模式，本文设计了一种基于液压驱动的机载式疏花机，并基于 ANSYS/LS-DYNA 的疏花过程动态仿真分析，探究疏花轴转速、行进速度及疏花半径对疏花击打力的影响规律。通过单因素与三因素三水平 Box-Behnken 试验建立疏花击打力回归模型，结果显示：疏花轴转速、行进速度、疏花半径对疏花击打力均有显著影响，且存在显著的交互作用；在疏花半径为 0.4m 时，对该模型求解确定最优参数组合为疏花轴转速 290r/min、行进速 度 5.4km/h，此参数下有效疏花范围在半径 0.4 ~0.6m 之间。为验证参数有效性，在半径为 0.4m 处对其进行仿真和室内台架对比试验，击打力分别为 5.083N 和 5.22N，误差率为 2.7%。田间试验结果表明，整机在最优参数下进行作业时，平均疏花率为 37.8%，在保障疏花率的同时显著降低了对枝叶的损伤。

INTRODUCTION
Flower thinning is a fundamental orchard management practice that regulates crop load, improves fruit quality, and maintains the nutritional balance of fruit trees *(Liu et al., 2018)*. However, manual thinning is inefficient and labor-intensive and has become increasingly incompatible with rising labor costs *(Liu et al., 2018; Gao et al., 2025; Hehnen et al., 2012; Si et al., 2024)*. Chemical thinning, although effective, is constrained by concerns over pesticide residues and environmental risks *(Lyons et al., 2015; Bound, 2021)*. As a result, mechanical thinning has emerged as an important development direction for modern orchards due to its high efficiency, low cost, and environmental friendliness *(Lei et al., 2019)*.

Since the 1980s, international research has focused on mechanical thinning devices based on trunk vibration and flexible striking mechanisms. Representative examples include the Darwin series developed in Germany, which uses centrifugal force to drive flexible ropes for flower removal *(Assirelli et al., 2018)*, and a comb-bar vibration thinner developed in the United States that reportedly reduced thinning costs by approximately 30% *(Schupp et al., 2008)*.

Yuliang Wang, Assoc. Prof. Ph.D. Eng.; Bowen GUO, M.S. Stud. Eng.; Zhaoying Chen, Ph.D. Stud. Eng.; Yuhao MA, M.S. Stud. Eng.; Guoqiang Fan, Assoc. Prof. Ph.D. Eng.; Jinxing Wang, Prof. Ph.D. Eng.

In recent years, intelligent technologies such as multispectral sensing and vision-based bud recognition have further improved thinning accuracy to over 90%. Nevertheless, most foreign equipment is poorly adapted to China's complex orchard environments and cultivation patterns. To address this limitation, domestic researchers have developed localized thinning devices *(Zhang et al., 2024)*, including a handheld rope-swing thinner with a rotational speed range of 0–900 r·min^{-1} *(Lei et al., 2020)*, a crawler-type self-propelled thinning machine *(Zhou et al., 2024)*, and a suspended electric flexible thinner incorporating ultrasonic sensing for canopy profiling *(Li et al., 2016)*. Despite these advances, the operating parameters of most existing machines are still determined primarily through field trial-and-error, with limited support from theoretical modeling and numerical simulation, making it difficult to achieve an optimal balance between thinning efficiency and tree protection.

Dynamic simulation provides an effective tool for the quantitative analysis and optimization of mechanical thinning parameters *(Sun et al., 2015; Liu et al., 2025)*. In particular, LS-DYNA is well suited for modeling transient impact processes and material nonlinearity, enabling accurate simulation of kinetic energy transfer and contact behavior between thinning ropes and flower-bearing branches *(Li et al., 2015; Cui et al., 2012)*. In this study, a hydraulic-controlled vehicle-mounted flower-thinning machine equipped with a steel wire rope–rubber composite thinning rope was developed to balance flexibility, strength, and durability. A rigid–flexible coupling model was established using ANSYS/LS-DYNA to quantify the effects of rotational speed, traveling speed, and thinning radius on the striking force. The optimal operating parameters were obtained through simulation and subsequently verified experimentally, providing a theoretical basis for the design and parameter optimization of orchard mechanical thinning equipment.

MATERIALS AND METHODS

Structure and working mechanism

Modern apple orchards commonly adopt a high-spindle planting mode, characterized by a trunk height of 70–80 cm, a tree height of approximately 3.5 m, an opening angle of 110–120°, a row spacing of 3.2–4.0 m, and a plant spacing of 0.8–1.0 m *(Wang et al., 2023)*. To ensure stable operation under these orchard conditions, the overall dimensions of the flower-thinning machine are 5.6 × 3.8 × 3.76 m (length × width × height).

The flower-thinning machine mainly consists of a tractor, a thinning mechanism, and a hydraulic system, as shown in Fig. 1. The thinning mechanism includes a rotating shaft mounting frame, a connecting bracket, and an attitude adjustment device, which is detachably connected to the tractor through a hanging bracket. The attitude adjustment device, composed of a longitudinal sliding sleeve and rail as well as a transverse sliding support, works in coordination with hydraulic cylinders to achieve precise multi-angle adjustment. The hydraulic system provides power to the hydraulic motor and cylinders, enabling both rotational motion and attitude adjustment of the thinning mechanism.

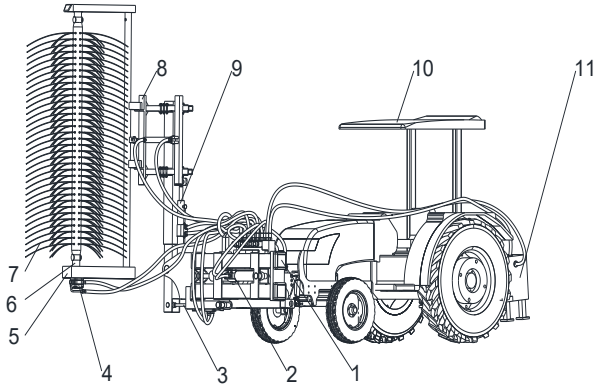

Fig. 1 - Schematic diagram of the overall flower-thinning machine

1 - Hydraulic valve group; 2 - Horizontal telescopic device; 3 - Angle adjustment device; 4 - Hydraulic motor; 5 - Flower-thinning device rotating shaft mounting frame; 6 - Flower-thinning shaft; 7 - Flower-thinning rubber strip; 8 - Flower-thinning device bracket; 9 - Vertical telescopic device; 10 - Tractor; 11 - Hydraulic station.

Table 1

Key Parameters of Flower-Thinning Machinery

Overall dimensions/m	Supporting power/KW	Thinning radius/m	Flower-thinning rope spacing/m	rotational speed range/r·min^{-1}	Tilt angle range/°
5.6×3.8×3.76	≥51.5	≥0.6	0.06	0–450	-15–15

The hydraulic system is the core component for attitude adjustment and power output. As shown in Fig. 2, a dual gear pump provides stable hydraulic pressure to the hydraulic cylinders and motor through the oil circuit. Precise control of the system is achieved using a three-position four-way solenoid valve group.

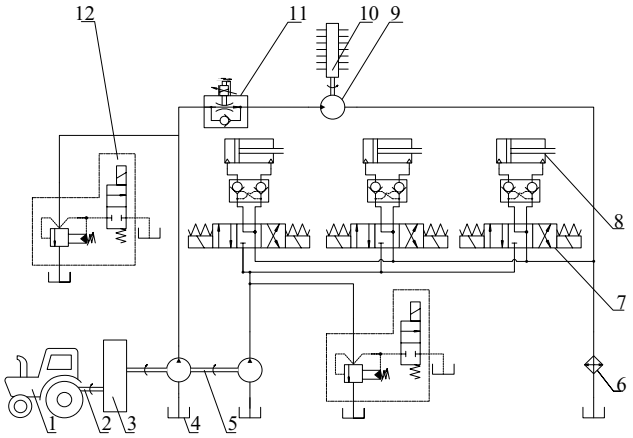

Fig. 2 - Schematic diagram of the hydraulic system

1 - Tractor; 2 - Rear power output shaft; 3 - Speed increasing device; 4 - Hydraulic oil tank; 5 - Dual gear pump; 6 - Radiator; 7 - Three-position four-way solenoid valve; 8 - Double-acting hydraulic cylinder; 9 - Cycloid hydraulic motor; 10 - Flower-thinning device; 11 - Electro-hydraulic proportional flow control valve; 12 - Pilot-operated electromagnetic relief valve.

The tractor provides mechanical, hydraulic, and walking power. Its rear axle connects to a hydraulic station, powering the hydraulic motor and cylinders. Solenoid valves control the thinning device's tilting and telescoping. After oil supply, the hydraulic motor drives the thinning shaft to rotate, making the thinning rope strike flowers via centrifugal force (Fig. 3). Different thinning effects are achieved by adjusting motor speed, traveling speed, rope spacing/type, and the mechanism's tilt angle.

Fig. 3 - Field operation of the orchard flower-thinning machine

Simulation and Analysis of Flower-Thinning Process

To investigate the flower-thinning process and clarify the breaking mechanism of flower stalks, apple flowers were selected as the test objects. The following assumptions were adopted: inflorescences were upright; flower stalks were homogeneous, flexible, and of equal diameter; thinning shafts were considered rigid; and external environmental interference was neglected. The collision between the thinning rope and the flower stalk was simplified as a nonlinear transient dynamic problem. The flexible stalk was modeled as a cantilever beam fixed at the base. When the bending stress generated by the external force reaches the ultimate strength of the stalk material, the stalk fractures. The maximum bending stress can be expressed as follows:

$$\sigma = \frac{32FL}{\pi d^3} \quad (1)$$

F - flower-thinning striking force, [N]

L - distance from point of application to base, [m]

d - the stalk diameter, [m]

The motion involves instantaneous flexible collision, large deformation at the free end, and rebound; therefore, inertial effects and collision velocity loads cannot be neglected in the analysis *(Cao et al., 2018)*. An explicit dynamic coupled solution was employed to solve the finite element model.

Healthy, pest-free apple flower samples collected on the same day were used for tensile tests conducted with a universal testing machine (Fig. 4a). Relevant physical parameters were measured using a high-precision electronic balance and vernier calipers, and each test was repeated at least eight times, with average values taken to ensure data reliability. Flower stalk density was determined using the water displacement method. During tensile testing, stress–strain data were recorded (Fig. 4b) to calculate Young's modulus, while axial elongation and transverse contraction were measured to determine Poisson's ratio.

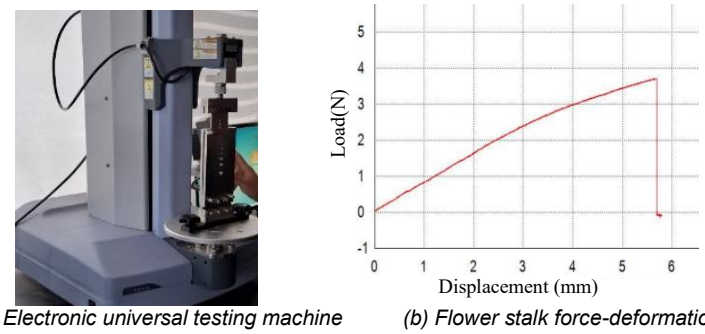

(a) Electronic universal testing machine *(b) Flower stalk force-deformation curve*

Fig. 4 - Determination of floral intrinsic parameters.

Statistical analysis of multiple tests showed that each apple inflorescence contains an average of six flowers. The average diameter of the apple receptacle and flower stalk were 3.6 mm and 1.8 mm, respectively. The mean density of apple flower stalks was approximately 1130 kg·m^{-3}, with a Young's modulus of about 9.53 MPa and a Poisson's ratio of 0.38, while the average mass of a single apple flower was 0.21 g. These material parameters provide a reliable basis for flower stalk force analysis and the establishment of the simulation model.

Because apple flowers contain numerous petals and must be defined as flexible bodies, direct modeling would result in a high computational burden. Therefore, in this study, each apple flower was simplified by attaching a mass point with the same weight as the flower to the free end of the flower stalk. In addition, to reduce computational complexity, non-critical components of the flower-thinning device were simplified, while key components such as the thinning shaft and thinning rope were retained. The simplified model is shown in Fig. 5, where v denotes the traveling speed of the flower-thinning device, n the rotational speed of the thinning shaft, ω the angular velocity, and R the thinning radius.

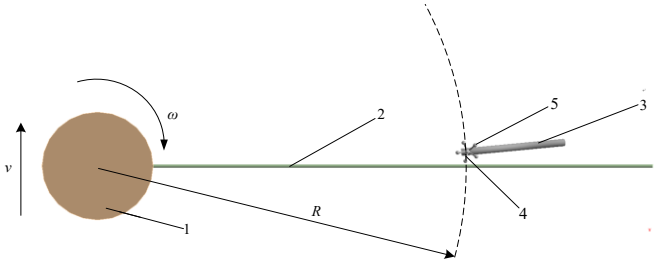

Fig. 5 - Rigid–flexible coupled dynamic model.

1 - Flower-thinning shaft; 2 - Flower-thinning rope; 3 - Fruit tree branch; 4 - Apple flower stalk; 5 - Flower mass point.

Modeling and assembly were completed in SolidWorks and then imported into LS-DYNA. Material properties were defined as follows: the flower stalk was modeled as a flexible body, and the flower-thinning shaft was treated as a rigid structural steel body. Meshing was performed with refined grids applied to the flower stalks. Boundary conditions included bonded contact between the shaft and rope, frictional contact between the rope and stalk (μ = 0.25, dynamic coefficient = 0.2, decay coefficient = 0.08), and fixed constraints on the branch surface. The traveling speed and rotational speed were set, and the simulation was executed. Contact force, displacement, and velocity curves were extracted to verify the rationality of the results, with validation against subsequent bench-test measurements and field thinning performance.

Simulation and Experimental Design

Previous tensile and shear tests showed flower stalks fracture at 3.5–5.5 N. Effective thinning requires the rubber strip to deliver at least 4.49 N *(Hu et al., 2015)*, while excessive force may damage branches and

reduce yield *(Quan et al., 2016)*. Therefore, a target striking force of 5 N was used in the simulations. Based on field investigations, the rotational speed, traveling speed, and thinning radius were identified as the main factors influencing the striking force. Single-factor simulation analyses were conducted to evaluate the effects of these parameters and determine the optimal combination, as summarized in Table 2.

Table 2

Factors and Levels of the Single-Factor Simulation Experiment

Test Group	Traveling speed/km·h⁻¹	Thinning radius/m	Rotational speed/r·min⁻¹
Test 1	0	0.5	210 ~ 450
Test 2	0	0.3 ~ 0.6	240
Test 3	5.2 ~ 16	0.5	210

The single-factor simulation results indicated that all three factors had significant effects on the striking force. Accordingly, a three-factor, three-level Box–Behnken response surface design (BBD) was adopted to evaluate the combined effects of these parameters and to determine the optimal parameter combination. The experimental factors and their coded levels are presented in Table 3.

Table 3

Coded Levels of Experimental Factors

Level	Rotational speed A/(r·min⁻¹)	Traveling speed B/(km·h⁻¹)	Thinning radius C/m
-1	210	5.2	0.3
0	345	10.6	0.45
1	480	16	0.6

RESULTS

Results of Single-Factor Simulation Test

The single-factor simulation results showed that the rotational speed, thinning radius, and traveling speed all significantly affected the striking force.

With the traveling speed and thinning radius held constant, simulations were conducted at different rotational speeds, and the resulting data were analyzed by regression to obtain the fitting curve and regression equation between rotational speed (n) and striking force (F):

$$F = 0.02057n - 0.5513 \tag{2}$$

F - striking force, [N]

n - flower-thinning rotational speed [r·min⁻¹])

As shown in Fig. 6(a) and the regression equation (2), within the range of 210–450 r·min⁻¹, the striking force increases markedly with rotational speed, indicating a strong positive correlation. At low rotational speeds, the striking force is insufficient for effective thinning, whereas excessive speed may cause damage to branches and leaves and increase energy consumption. Therefore, the optimal rotational speed range was determined to be 210–480 r·min⁻¹, ensuring thinning efficiency while reducing damage to fruit trees.

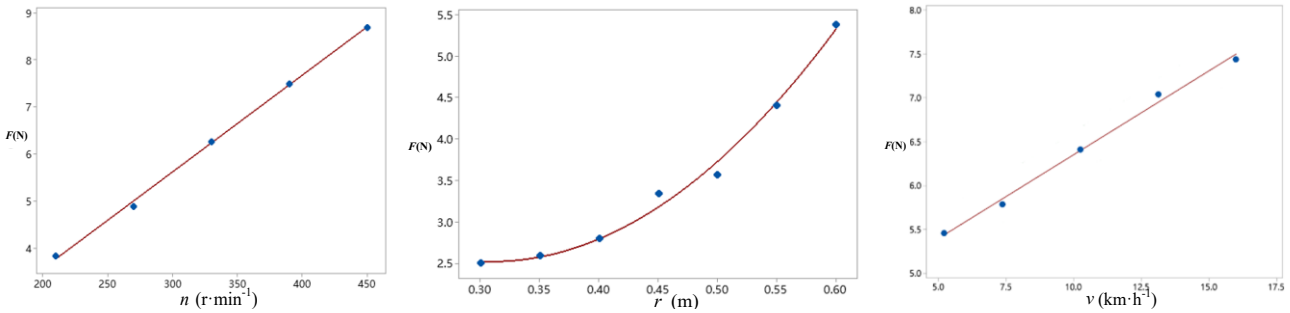

(a) Striking force vs. rotational speed *(b) Striking force vs. thinning radius* *(c) Striking force vs. traveling speed.*

Fig.6 Influence of each factor on striking force.

With the rotational speed and traveling speed held constant, the effect of different thinning radii on the striking force was investigated. Regression analysis was performed to obtain the regression equation and fitting curve between the thinning radius (r) and striking force (F):

$$F = 5.699 - 20.54r + 33.20r^2 \tag{3}$$

r – thinning radius, [m]

As shown in the fitting curve in Fig. 6(b) and the regression equation (3), when the thinning radius decreases from 0.6 m to 0.3 m, the striking force decreases rapidly and approaches zero. When the thinning position is closer to the shaft end, the motion range of the rope tip and its kinetic energy are limited, resulting in a lower striking force. In contrast, the swing amplitude and kinetic energy at the rope end are the largest, leading to higher thinning efficiency. Therefore, a thinning radius range of 0.3–0.6 m was selected for subsequent experiments, which ensures sufficient striking force and thinning effectiveness while avoiding excessive impact on branches and leaves.

With the rotational speed and thinning radius held constant, the effect of traveling speed on the striking force was investigated. Regression analysis was conducted to obtain the regression equation and fitting curve between traveling speed (v) and striking force (F):

$$F = 4.445 + 0.1908v \tag{4}$$

v – traveling speed, [km · h⁻¹]

As shown in the fitting curve in Fig. 6(c) and the regression equation (4), within the traveling speed range of 5.2–16 km·h⁻¹, the striking force exhibits a positive correlation with increasing speed. This is because higher traveling speed increases the linear velocity of the flower-thinning rope and enhances its kinetic energy, thereby improving the striking effect. Excessively high speed may cause unstable operation and increase operational risk, whereas excessively low speed results in insufficient thinning efficiency. Therefore, the traveling speed range was determined to be 5.2–16 km·h⁻¹.

Analysis of Multi-Factor Simulation Test Results

Based on the Box–Behnken response surface design, simulation tests were conducted to evaluate the combined effects of multiple factors on the striking force following the single-factor analysis and to determine the optimal parameter combination. The test factors included the rotational speed, travelling speed, and thinning radius, with striking force as the evaluation index. The experimental design matrix and simulation results are presented in Table 4.

Table 4

Experimental design matrix and simulation results.

Test Group	A/(r·min⁻¹)	B/(km·h⁻¹)	C/m	Striking force/N
1	345	10.6	0.45	7.6456
2	210	10.6	0.3	2.6768
3	345	16	0.6	13.363
4	345	5.2	0.3	2.9762
5	480	16	0.45	11.104
6	345	10.6	0.45	7.4894
7	210	5.2	0.45	3.9478
8	480	10.6	0.6	13.503
9	210	10.6	0.6	7.8375
10	210	16	0.45	5.9378
11	480	10.6	0.3	1.7629
12	345	5.2	0.6	9.265
13	345	10.6	0.45	7.7901
14	480	5.2	0.45	7.0085
15	345	16	0.3	3.9786
16	345	10.6	0.45	8.312
17	345	10.6	0.45	7.7201

Based on the data in Table 4, a response surface regression model describing the effects of rotational speed, traveling speed, and thinning radius on the striking force was established using Design-Expert 13.0. A quadratic polynomial regression equation for the striking force was obtained as follows:

$$F = 7.79 + 1.62A + 1.39B + 4.07C + 0.53AB + 1.64AC + 0.77BC - 0.87A^2 + 0.08B^2 - 0.48C^2 \tag{5}$$

As shown by the analysis of variance results in Table 5, the regression model exhibits a P value lower than 0.0001, indicating that the model is highly significant. The lack-of-fit term has a P value greater than 0.05, suggesting that the lack of fit is not significant and that the model shows good agreement with the data.

All three factors—rotational speed, traveling speed, and thinning radius—have extremely significant effects on the striking force, with the influence ranking from highest to lowest being thinning radius, rotational speed, and traveling speed. Regarding interaction effects, the interactions between rotational speed and thinning radius and between traveling speed and thinning radius are significant ($P < 0.05$), whereas the interaction between rotational speed and traveling speed is not significant. In addition, the quadratic term of rotational speed has a significant effect on the striking force. The coefficient of determination (R^2) and adjusted R^2 of the model are 0.988 and 0.973, respectively, and the low coefficient of variation indicates high model reliability, providing a sound basis for subsequent parameter optimization.

Table 5

Analysis of Variance of the Quadratic Polynomial Model for Striking Force.

Source	Squares	DF	MS	F value	P value
Models	188.00	9	20.89	66.22	< 0.0001
A	21.06	1	21.06	66.75	< 0.0001
B	15.64	1	15.64	49.59	0.0002
C	132.63	1	132.63	420.49	< 0.0001
AB	1.11	1	1.11	3.51	0.1030
AC	10.82	1	10.82	34.31	0.0006
BC	2.40	1	2.40	7.60	0.0283
A²	3.20	1	3.20	10.13	0.0154
B²	0.0265	1	0.0265	0.0841	0.7802
C²	0.9504	1	0.9504	3.01	0.1262
Residual	2.21	7	0.3154		
Lack of Fit	1.82	3	0.6065	6.24	0.0545
Source	**Squares**	**DF**	**MS**	**F value**	**P value**
Pure Error	0.3886	4	0.0971		
Cor Total	190.21	16			

Note:P<0.01(extremely significant,**), P<0.05(significant,*)

The response surface plots (Fig. 7) show that, at a fixed thinning radius, the striking force increases gradually with increasing rotational speed and traveling speed. When the traveling speed is fixed, both thinning radius and rotational speed exhibit significant positive correlations with the striking force, and the uniform spacing of the contour lines at the lower region indicates a relatively smooth variation trend. With rotational speed held constant, the influence of thinning radius on the striking force is much greater than that of traveling speed; moreover, at a constant traveling speed, the striking force increases with increasing thinning radius.

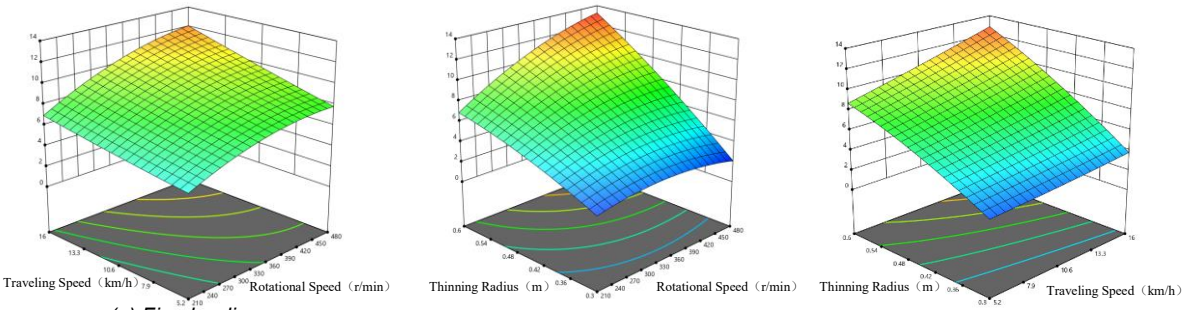

(a) Fixed radius *(b) Fixed traveling speed* *(c) Fixed ratational speed*

Fig. 7 - Response surface of interaction effects

Parameter Optimization

Using Design-Expert 13.0's Optimization function, optimal parameters at C=0.4m (target F=5N) were: A=290r/min, B=5.4km/h. To quantify the flower-thinning intensity and verify the rationality of the optimized parameters, the Integrated Coefficient of Thinning (ICT) *(Solomakhin et al., 2010)* was introduced to evaluate the balance between thinning efficiency and tree protection, and its expression is given as follows:

$$ICT = \frac{m \times s^2}{F_s \times v \times r} \quad (6)$$

Fs – absolute fruit set rate [%]

m – mass of a single flower-thinning rope [kg]

S – rotational speed [r/min]

When the ICT value ranges from 10 to 40, the thinning operation is considered effective; values above 50 indicate potential damage to fruit trees, while values below 8 correspond to poor thinning quality. By substituting the parameters into Eq. (5) (s = 290 r·min^{-1}, v = 5.4 km·h^{-1}, r = 0.6 m to evaluate upper range limit), together with the field-measured fruit set rate F_S = 34.4%, the average from 20 representative branches in the test orchard, and m = 0.03 kg, the calculated ICT value was 22.64. This value falls within the effective operation range of 10–40, indicating that the selected parameter combination ensures satisfactory thinning performance while effectively controlling the risk of mechanical damage to the tree.

To verify the reliability of the optimal parameters, simulation and indoor bench comparison tests were conducted under the selected operating conditions. The simulation results are shown in Fig. 8. When the flower-thinning rope comes into contact with the flower stalk, the striking force rapidly increases from 0 to a peak value of 5.083 N, and then drops sharply to zero after the stalk is broken. As shown in Fig. 9, four out of six flower stalks in a single inflorescence were fractured in the simulation, indicating that the flower-thinning rope exhibits good striking and stalk-breaking performance under the optimized parameters. These results provide a reliable basis for subsequent field tests and further parameter optimization.

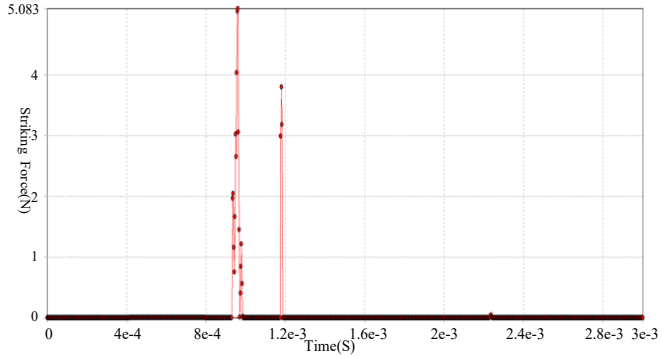

Fig. 8 - The striking force under optimal parameters

Fig. 9 - Flower-thinning process under optimal parameters

An indoor test bench was established to measure the striking force of the flower-thinning rope and verify the reliability of the optimal parameters. Two dynamometers with fixed spacing and peak-hold capability were installed, with a force-bearing rod horizontally fixed below them. Under the optimal operating conditions, the flower-thinning rope struck the force-bearing rod, and the striking force was obtained from the dynamometer readings. The comparison results are presented in Table 6. At a thinning radius of 0.4 m, the measured striking force was 5.22 N, with an average error of only 2.7% compared with the simulation result. The results indicate that when the thinning radius exceeds 0.4 m, the striking force remains above 4.49 N, and the variation trends of striking force from simulation and indoor tests are consistent, confirming an effective thinning radius range of 0.4–0.6 m under the optimized parameters.

Table 6

Comparison between simulation and experimental results under optimal parameters.

Serial Number	Thinning radius/m	Striking force /N		Error rate/%
		Trial value	Simulation value	
1	0.3	1.89	1.71	9.5
2	0.4	5.22	5.08	2.7
3	0.5	7.21	6.83	5.3
4	0.6	7.79	8.32	4.5

Field Test

To verify the flower-thinning performance of the vehicle-mounted flower-thinning machine under optimal operating parameters, as well as the rationality of the structural design and component selection, field tests were conducted in mid-April 2025 at the China–Netherlands Demonstration Base in Songxingtun Village, Kanjia Town, Yantai City, Shandong Province, China.

The test orchard was planted with 3–5-year-old apple trees, with row spacing of 3.2–4.0 m and tree heights ranging from 3.2 to 3.5 m. Prior to testing, the flower-thinning machine was adjusted to ensure stable and normal operation of all mechanisms. The flower-thinning rate was calculated by recording the number of flowers before and after thinning:

$$C = \left(1 - \frac{N_0}{N}\right) \times 100\% \tag{7}$$

C – flower thinning rate [%]

N_0 – number of remaining flowers after operation

N – initial number of flowers

Ten apple trees were randomly selected in the orchard, and one representative branch from each tree was chosen as a sampling point. Flower-thinning operations were carried out under the optimal parameter conditions. The apple inflorescences before and after thinning are shown in Fig. 10, and the corresponding test data are presented in Table 7.

Fig. 10 - Comparison of apple flower clusters before and after thinning

Table 7

Field test data of the flower-thinning machine.

Initial number of flowers N/flower	Number of remaining flowers N_0/flower	Flower thinning rate C/%
39	26	33
28	11	31
28	18	36
33	20	39
18	10	44
34	21	38
39	23	41
21	12	43
17	11	35
21	13	38

Under the optimal parameter combination, field tests of the flower-thinning machine yielded an average thinning rate of 37.8% (standard deviation 4.2%), with all samples exceeding 30%. Compared with manual thinning performed during the same period, the mechanical method satisfied agronomic requirements while maintaining low levels of damage to branches and leaves, and significantly improved operational efficiency by reducing labor costs. It operated stably throughout the thinning process, demonstrating that the overall design meets operational requirements and is capable of fulfilling orchard flower-thinning demands.

CONCLUSIONS

A hydraulic-controlled vehicle-mounted flower-thinning machine was developed specifically for China's dwarf and dense planting orchards. The machine, with overall dimensions of 5.6 × 3.8 × 3.76 m and an adjustable structural design, meets the operational requirements of most orchard conditions and exhibits improved adaptability compared to existing rope-swing and trunk-vibration thinners.

Explicit dynamic simulation results demonstrate that the striking force is significantly positively correlated with the rotational speed of the thinning shaft, traveling speed, and thinning radius. A quadratic regression model established based on the multi-factor experimental design shows a high degree of fit (R^2 = 0.988), indicating that the thinning radius has the most pronounced effect on the striking force, followed by rotational speed and traveling speed. The optimal parameter combination was obtained by solving the regression model. Under these optimized parameters, ANSYS simulation and indoor bench tests produced striking forces of 5.08 N and 5.22 N, respectively, with a relative error of 2.7% and consistent variation trends. Field experiments further confirmed that the thinning rate of all selected samples exceeded 30%, with an average thinning rate of 37.8%.

Future research may further investigate the nonlinear contact behavior and energy transfer characteristics between flexible thinning elements and fruit tree branches. In addition, intelligent control technologies could be integrated to enable real-time adjustment and adaptive control of thinning operation parameters, thereby enhancing the intelligence level and engineering applicability of mechanical flower-thinning equipment.

ACKNOWLEDGEMENT

This work was supported by “China Agriculture Research System of MOF and MARA (CARS-27) and Shandong Province Key Research and Development Plan (2022CXGC020706)”.

REFERENCES

[1] Assirelli A., Giovannini D., Cacchi M., Sirri, S., Baruzzi, G., Caracciolo, G. (2018). Evaluation of a new machine for flower and fruit thinning in stone fruits. *Sustainability*, 10(11), 4088. DOI:10.3390/su10114088.

[2] Bound S.A. (2021). Managing crop load in European pear (*Pyrus communis L.*) — A review. *Agriculture*, 11(7), 637. DOI:10.3390/agriculture11070637.

[3] Cao, W.B., Sun, W.L., Niu, C., Jiao, H.B., Chen, B.B. (2018). Combed safflower picking device based on ANSYS/LS-DYNA. *Transactions of the Chinese Society for Agricultural Machinery*, 49(11), 123–131.

[4] Cui, T., Liu, J., Zhang, D.X., Shi, S. (2012). Flexible body simulation for corn stem based on ANSYS and ADAMS. *Transactions of the Chinese Society for Agricultural Machinery*, 43(S1), 112–115.

[5] Gao, A., Wu, K., Song, Y.P., Ren, L.L., Ma, W., Liu, Y.L. (2025). Parameter optimization and experiment of apple laser thinning test bench based on LT-YOLO detection and machine vision. *Transactions of the Chinese Society for Agricultural Machinery*, 56(02), 393–401.

[6] Hehnen, D., Hanrahan, I., Lewis, K., McFerson, J., Blanke, M. (2012). Mechanical flower thinning improves fruit quality of apples and promotes consistent bearing. *Scientia Horticulturae*, 134, 241–244.

[7] Hu, C.Q., Sun, C.H., Xu, Y. (2015). Experiment and analysis of mechanical properties for branches–pedicel node and receptacles–corolla node of apple tree. *Journal of Qingdao Agricultural University (Natural Science)*, 32(03), 211–214.

[8] Lei, X.H., Lv, X.L., Zhang, M.N., Ma, X.L., Chang, Y.H., Herbst, A. (2019). Development and test of three-arms tractor-mounted flower thinner. *Transactions of the Chinese Society of Agricultural Engineering*, 35(24), 31–38.

[9] Lei, X.H., Lv, X.L., Zhang, M.N., Ma, X.L., Chang, Y.H., Herbst, A. (2020). Experimental study on electric rope-swing thinning machine in Cuiguan pear orchard. *Journal of Chinese Agricultural Mechanization*, 41(9), 47–52.

[10] Li, J., Xu, Y., Xu, J.T., Yang, Z., Lu, H.Z. (2016). Design and experiment of control system for suspended electric flexible thinner. *Transactions of the Chinese Society of Agricultural Engineering*, 32(18), 61–66.

[11] Li, X.D., Fang, X.F., Han, Z.D., Zhang, Z.R., Liu, G.M., Cui, J.W., Qiao, X.D., Han, K.L. (2015). Dynamic simulation of rotary cutter for sweet sorghum based on ANSYS/LS-DYNA. *Journal of Agricultural Science and Technology*, 17(03), 70–76.

[12] Liu, H.W., Chi, J.K., Liang, Q.J., Liu, T.Y., Wang, H.L., Li, S.D., Hu, C.Q. (2025). Design and simulation analysis of crawler-type double-arm apple flower thinning machine. *Journal of Agricultural Mechanization Research*, 47(06), 35–41.

[13] Liu, L.M., Nie, L., Zhao, H.L., Cao, Y.J., Sun, A. (2018). Study on apple flower and fruit thinning technology. *Shanxi Journal of Agricultural Sciences*, vol.64, no.11, 88–91.

[14] Lyons, D.J., Heinemann, P.H., Schupp, J.R., Baugher, T.A., Liu, J. (2015). Development of a selective automated blossom thinning system for peaches. *Transactions of the ASABE*, 58(6), 1447–1457.

[15] Quan, P.K., Li, Y.C., Zhang, S.J., Wang, T., Song, X., Zhang, Z.X. (2016). Study on mechanical properties of apple tree branches during maturity season. *Journal of Chinese Agricultural Mechanization*, (10), 44–47.
[16] Schupp, J.R., Baugher, T.A., McClure, B.A., Harsh, R.M., Lesser, K.M. (2008). Mechanical thinning of peach and apple trees reduces labor input and increases fruit size. *HortTechnology*, 18(4), 660–670.
[17] Si, Y.S., Kong, D.H., Wang, K.J., Liu, L.X., Yang, X. (2024). Recognition method of central and peripheral apple flowers based on CRV-YOLO. *Transactions of the Chinese Society for Agricultural Machinery*, 55(02), 278–286.
[18] Solomakhin A.A., Blanke M.M. (2010). Mechanical flower thinning improves the fruit quality of apples, *Journal of the Science of Food and Agriculture*, vol.90, 735–741.
[19] Sun, C.H., Hu, C.Q., Hou, Q.S., Pan, Z.G. (2015). Simulation analysis of the mechanical flexible thinning machine actuator based on ADAMS. *Journal of Agricultural Mechanization Research*, 37(12), 70–73. DOI:10.13427/j.cnki.njyi.2015.12.017.
[20] Wang, Y.L., Wang, Z.Q., Chen, Z.Y., Fan, G.Q., Su, R., Yin, P.J., Wang, J.X. (2023). Design and testing of modern apple orchard pruning machinery. *INMATEH - Agricultural Engineering*, 71(3), 93–102.
[21] Zhang, Z., Lei, X.H., Wang, W., Herbst, A., Lv, X.L. (2024). Research progress on mechanized thinning technology and equipment in orchards. *Journal of Chinese Agricultural Mechanization*, 45(10), 344–352.
[22] Zhou, Y., He, L., Song, L., Pan, Y.F., Wang, Q., Song, Z.S. (2024). Design and experiment of self-propelled track flower-thinning machine in orchards. *Xinjiang Agricultural Sciences*, 61(10), 2514–2526.